Journal of Metals, Materials and Minerals, 36(1), e2301, 2026

Mechanical properties and crystallization of polybutylene terephthalate reinforced with glass flakes and aluminum powder

Nattakarn HONGSRIPHAN[1,*], and Pajaera PATANATHABUTR[1]

[1] *Department of Materials Science and Engineering, Faculty of Engineering and Industrial Technology, Silpakorn University, Nakhon Pathom, 73000, Thailand*

***Corresponding author e-mail**: Hongsriphan_N@silpakorn.edu

Received date:
29 April 2025
Revised date:
2 July 2025
Accepted date:
30 October 2025

Keywords:
PBT;
Glass flake;
Aluminum powder;
Electrical surface resistivity;
Composite

Abstract

This research investigated mechanical properties and crystallization of poly(butylene terephthalate) composites by adding glass flakes (GF) and aluminum particles (Al). The concentration of the GF was 3 wt% or 5 wt%, and the Al was 0.5 wt% or 1.0 wt%. The stress-strain curves of the PBT-based composites showed yielding and necking. The PBT/GF/Al composites with GF/Al ratios of 3/0.5 wt/wt%, 3/1.0 wt/wt%, 5/0.5 wt/wt%, and 5/1.0 wt/wt% had Young's moduli of 11.44%, 11.70%, 16.81%, and 19.31% higher than that of neat PBT, respectively. In the presence of Al at 1.0 wt%, the flexural modulus of the PBT/GF/Al composites increased to 3.6% higher than that of neat PBT, and all flexure specimens recovered elastically after being subjected to 5% strain. The neat PBT and all PBT/GF/Al composites exhibited the XRD pattern of α-form crystals, in which the changed crystal dimensions implied the heterogeneous nucleation with the presence of these fillers. The cooling rate of the injection molding was so fast that the filler-nucleated crystallization formed only α-form crystals. Adding the GF and Al increased the T_c of the PBT matrix, confirming these fillers acted as nucleating agents. Adding GF/Al fillers of 6 wt% reduced the electrical surface resistivity to 10^{10} ohm·sq^{-1}, indicating it was an anti-static material.

1. Introduction

Poly(butylene terephthalate) (PBT) [1,2] is an engineering thermoplastics made from terephthalic acid and 1,4-butanediol, which offers interesting properties such as stiffness, excellent dimensional stability, good resistance to chemicals, desirable electrical properties, wear resistance, and easy processability. It is a polyester that can crystallize gradually during the cooling process and provides these properties. They have been used in various of applications to obtain products by extrusion (i.e. toothbrush bristles, PBT films for electrical or medical purposes) and injection molding (bearings and bushings, electrical and electronic devices, automotive parts, and food processing machinery components). PBT is considered the main polyamide competitor because its mechanical properties are better than polyamides due to its much lower moisture uptake and better dimensional stability properties under wet conditions. The injection-molded PBT items have improved mechanical performance by reinforcing with fillers or fibers [3,4]. This is due to easy molding and fast crystallization of the PBT composites. PBT crystallizes in two forms, namely the α-form and the β-form crystals [5], and both of them are triclinic crystal systems. When PBT melt is cooled down, the molecules nucleate and the α-form crystals are grown. Meanwhile, the β-form crystals are obtained upon mechanical deformation (i.e., uniaxial stretching of about 5% to 15% strain) [6] of PBT in the α-form crystal. However, these β-form crystals are not stable, and after stress relaxation, the α-form crystals are normally recovered. Technically, the pain point of the PBT processing is based on the thermo-oxidative degradation of the polyester linkage. The concern with melt compounding of the PBT matrix with inorganic fillers containing high oxygen content is the residual moisture that can cause voids inside the molded parts or excessive reduction in melt viscosity during processing.

Glass flake (GF) is an extremely thin platelet glass with various particle size distributions and aspect ratios [7] that is manufactured by the bubble method or centrifugal method [8]. GF is applied in a wide range of applications, giving improvement for barrier properties, mechanical properties, and thermal properties. There are several research studies [9,10] that GF has been used as a reinforcing filler in epoxy resin or polyester resin aiming to produce a corrosion-protective coating. Alagöz and Selver [11] improved the seawater degradation of the epoxy resin by placing GF (50 μm in size) in various ratios (5% to 15%) on the surfaces of the glass fiber/epoxy composite material. They found that the use of GF improved the residual strength values after exposure to seawater for a period ranging from 0 month to 12 month. This was due to GF preventing water penetration. GF has also been mixed with thermoplastics to produce composites with enhanced mechanical properties [12], good transparency [13], or improved shrinkage/part warpage [14]. Vidakis *et al.* [15] produced composite filaments by melting compounding poly(lactic acid) and glass in powder, bead, and flake forms at various loadings. They concluded that all three glass forms influenced high reinforcement effects (up to 60% in flexural loading), especially in the flake form.

Electrically conductive plastics are divided into two segments: enhanced but still low conductivity for electrostatic-charge dissipating applications and high conductivity for electromagnetic-interference

shielding [16]. Investigations have shown that metal-filled polymers exhibit insulating properties until the percolation threshold concentration of conductive filler is achieved. Several literature studies [17,18] report the possibility of using aluminum particles as the conductive filler since they show great electrical and thermal conductivity due to high intrinsic electrical conductivity, coupled with a relatively low cost. For aluminum-filled polymers, it was found that the sudden and large reduction of the electrical surface resistivity occurred in the concentration of 15 vol% to 30 vol%. When adding metal particles in a concentration lower than 15 vol%, the electrical surface resistivity was reduced gradually in the range of 10^{12} ohm·sq^{-1} to 10^{14} ohm·sq^{-1} which could be used for designing the electrostatic-charge dissipating products. Recently, Alhamidi *et al.* [10] compounded Al nanoplatelets of 25 vol% into the PBT/PET 60/40 wt% blend and reported that the composite had the electrical resistivity of 7.2 ohm·cm^{-1} × 10^7 ohm·cm^{-1}, which was in the category of an electrostatic-charge dissipation material. The applications of the PBT-based composites [19] are sensor housings, automotive ECU and ADAS/sensor applications, terminal boards, etc.

This research was aimed to investigate mechanical properties and crystallization of PBT reinforced with GF and Al particles in a maximum concentration of 6 wt%. Since the crystallization of PBT was well-known to be affected by the injection molding condition, narrow-necked tensile specimens were used to investigate mechanical properties and their crystallization. This kind of the molded specimen is not common in the research work, only used for the study of the relationship between the processing condition and the flow-induced crystallization of the semi-crystalline polymer. Crystallization of the injection-molded specimens was also evaluated by the X-ray diffraction and the differential scanning calorimeter. The morphology of the cryo-fractured surface was studied via the scanning electron microscope. Finally, the electrical property of the injection-molded specimens was measured by an electrical surface resistivity meter.

2. Materials and experimental

2.1 Materials

Poly(butylene terephthalate) (Crastin® PBT S600F20, injection molding grade, melting temperature of 220°C) was purchased from DuPont Performance Polymers, USA. It had a melt flow index of 17.70 at 245°C using a loading weight of 2.16 kg. Glass flake (GF) and aluminum particles (Al) were kindly provided by the Concrete Composite Co., Thailand, and they were used as received.

2.2 Composite compounding

Prior to melting compounding, PBT pellets, glass flake (GF), and aluminum (Al) particles were dried thoroughly in an air-circulating oven at 120°C (6 h), 100°C (12 h), and 100°C (12 h), respectively. The composition of the composites is shown in Table 1. Glass flakes (GF) and aluminum particles (Al) were premixed by weighing and shaking together in a small plastic bag, and then poured into a bag of warm PBT pellets and shaking. The premixed compositions were kept in a sealed plastic box having silica gel.

The melting compounding was carried out using a twin-screw extruder (SHJ-25, Nanjing Youngteng Chemical Equipment, China). The processing temperature profile was set from the feed zone to the die zone in the temperature range of 240°C to 260°C, and the screw speed was set constant at 140 rpm. The melt extrudate was water-cooled and then pelletized by a pelletizer.

2.3 Injection molding of specimens

The PBT100 and PBT-based composite pellets were dried in an air-circulating oven at 120°C for 6 h. This ensured that the hydrolysis occurring during the injection molding process was neglected as tested by Loyer *et al.* [20]. The tensile specimens were injection-molded using an injection molding machine (SmartPower 35/210 UNILOG B8, Wittmann Battenfeld, Thailand). The barrel temperature profile was kept constant at 240°C to 260°C, and the nozzle temperature was set at 260°C to 270°C depending on the filler concentration. The mold temperature was kept at 80°C, which was the recommended mold temperature for good dimensional stability. The injection velocity and the packing/holding time were set constant. The cooling time was also kept constant at 30 s. Figure 1 presents injection-molded specimens with narrow-necked gauge lengths for tensile testing and rectangular specimens for flexural testing.

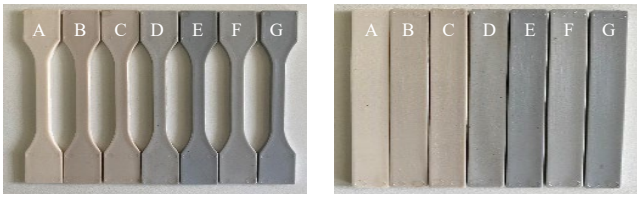

Figure 1. Injection-molded specimens of PBT100 (a), PBTGF3Al0 (b), PBTGF5Al0 (c), PBTGF3Al05 (d), PBTGF5Al05 (e), PBTGF3Al10 (f), and PBTGF5Al10 (g).

Table 1. Abbreviations and compositions of neat PBT and PBT composites.

Abbreviation	PBT pellets [wt%]	Glass flakes [wt%]	Aluminum particles (wt%)
PBT100	100.0	0	0.0
PBTGF3Al0	97.0	3	0.0
PBTGF5Al0	95.0	5	0.0
PBTGF3Al05	96.5	3	0.5
PBTGF5Al05	94.5	5	0.5
PBTGF3Al10	96.0	3	1.0
PBTGF5Al10	94.0	5	1.0

2.4 Characterization and testing

Tensile testing was carried out in accordance with ASTM-D638 using a universal testing machine (Instron model 5969, Instron Engineering Corporation, USA). Tensile specimens had narrow-necked gauge lengths in order to enhance the flow-induced crystallization. The tensile testing was performed using a crosshead speed of 50.8 mm·min^{-1} with a load cell of 5 kN. Eight specimens of each composition were tested, and the averages and the standard deviations were reported.

Flexural testing was carried out in accordance with ASTM-D790 using a universal testing machine (Instron model 5969, Instron Engineering Corporation, USA). Rectangular specimens (12.60 mm × 3.00 mm) were tested with the three-point bending mode using a strain rate of 0.01 (crosshead speed of 1.365 mm·min^{-1}). The span length was set at 51.2 mm. The load cell of 5 kN was used. The averages and standard deviations of six measurements were calculated and reported.

For tensile and flexural testing results, the one-way ANOVA with a 95% confidence ($p < 0.05$) was performed to analyze statistically the significant difference between group means, and followed by the post-hoc test (Tukey pairwise multiple comparisons) to provide a letter for each group. If two groups of results have different letters (e.g., "a" and "b"), it indicates a statistically significant difference between their means. The statistical calculation was performed with the help of Google Gemini after using Microsoft® Excel for the one-way ANOVA.

The cross-sectional surface of cryo-fractured specimens was examined using a FE-SEM/EDS (Tescan, Mira 3 , Czech Republic). The surface was platinum-gold coated prior to inspection to avoid electrostatic charging.

The XRD patterns of PBT100 and PBT/GF/Al composites were performed using a diffractometer (Rigaku, Miniflexll, Japan) with a Cu Kα anode (λ = 0.1540598 nm) and a rotating anode generator operated at 40 kV and 8 mA from 10° to 40°. The scan step side was 0.02° per step and a dwell time of 18.87 s per increment. The samples were cut from the skin area of the injection-molded specimens. The crystallite size of PBT was calculated using the Scherrer equation as follows.

$$L_{hkl} = \frac{K\lambda}{\beta_{hkl} \cos \theta_{hkl}} \quad (1)$$

where L_{hkl} was the crystallite size, characterizing [hkl] plane; K was the Scherrer constant (0.9); βhkl was the width at half height; λ was X-ray wavelength; and θ was the Bragg angle.

The molded specimens of each composition were cut into small pieces (4 mg to 5 mg) for thermal property analysis by a differential scanning calorimeter (DSC Pyris 1, Perkin Elmer, USA). The DSC samples were cut at the skin and the core area from the gauge area of the narrow-necked tensile specimen as shown in Figure 2.

The tests were performed in a heat-cool-reheat mode from 50°C to 260°C with a heating/cooling rate of 10°C·min^{-1}. The crystal melting temperature (T_m), the crystallization temperature (T_c), and the degree of crystallinity (X_c) were reported. The degree of crystallinity (X_c) was calculated using the following equation:

$$\%x_c = \frac{\Delta H_m}{\Delta H_f^o} \times \frac{100}{w} \quad (2)$$

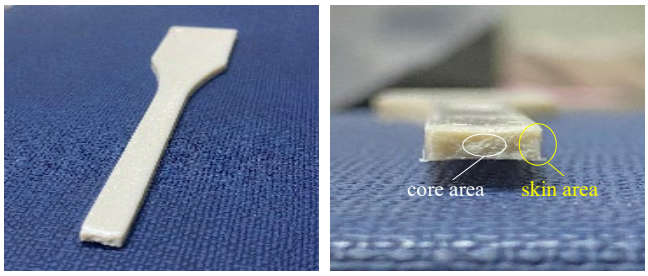

Figure 2. The DSC samples were cut at skin and core area from the gauge area of the narrow-necked tensile specimen.

where ΔH_m was melting enthalpy of crystalline (J·g^{-1}), ΔH_f^o was melting enthalpy of 100% crystalline of PBT (140 J·g^{-1}) [21], and w was weight fraction of PBT in composites.

Non-isothermal crystallization was performed as follows. The samples were rapidly heated from 40°C to 240°C at 80°C·min^{-1}, and the samples were maintained at 240°C for 5 min to erase their thermal history. Subsequently, the samples were cooled to 50°C at the cooling rates of 20°C·min^{-1}, 30°C·min^{-1}, 40°C·min^{-1}, 50°C·min^{-1}, and 60 °C·min^{-1}, which was different from the heating/cooling rate of 10 °C·min^{-1} of the previous DSC analysis. The exothermic curves of heat flow as a function of temperature were recorded, and the crystallization temperature of the PBT100 and the PBT/GF/Al composites were determined and compared.

Electrical surface resistivity of PBT100 and PBT/GF/Al composites was measured by a surface electrical resistance meter (BFN-TR1380, Thailand). Ten molded specimens were measured, and the averages were reported.

3. Results and discussion

3.1 Tensile properties of PBT100 and PBT/GF/Al composites

Figure 3 presents tensile properties of PBT100 and PBT/GF/Al composites, while Table 2 summarizes Young's modulus, tensile strength & elongation at maximum stress, and tensile strength & elongation at break of PBT100 and PBT/GF/Al composites. In this study, the injection-molded PBT100 or neat PBT specimens had Young's modulus of 259.04 MPa. As shown in Figure 3(a), adding GF of 3 wt% or 5 wt% increased Young's modulus of the PBT-based composites, and the increased percentage of the PBT-based composite adding GF of 3 wt% and 5 wt% was higher than that of neat polymer 8.24% and 12.94%, respectively. Hamlaoui *et al.* [22] reported that the increased modulus of the PBT adding glass fibers of 5 wt% was about 10.28% under the tensile crosshead velocity of 5 mm·min^{-1}.

Adding Al particles of 0.5 wt% and 1.0 wt% further increased Young's modulus to be higher 11.44% and 11.70% for the PBT-based composites adding GF of 3 wt%, and to be higher 16.81% and 19.31% for the PBT-based composites adding GF of 5 wt%. The mechanical enhancement of metallic particles is significantly improved compared with the filler concentration. Figure 3(b) presents the trend line of the enhancement of Young's modulus for the PBT-based composites with the addition of Al particles in the linear relationship between the tensile modulus and the filler concentration. When incorporating

the Al particles of only 0.5 wt% or 1.0 wt%, the slope values of the trend line increased significantly. This implies the good distribution of metallic particles in the PBT polyester matrix. These particles nucleate the crystals of the PBT matrix and restrict the mobility of the PBT molecules when the composites are subjected to tensile loading.

Figure 3(c-d) present tensile strength and elongation at maximum stress and at break of the PBT100 and the PBT/GF/Al composites, respectively. The typical stress-strain curves of the PBT100 specimens presented yielding [20] that the tensile strength at yield was the highest with the value of about 29 MPa. The elongation at break of the PBT100 specimens was about 233%. The elongation at break of the PBT/GF/Al composites was decreased to be in the range of 40% to 60% when reinforcing with the GF/Al fillers of around 6 wt% in this study. The stress-strain curves of the PBT adding GF of 3 wt% or 5 wt% still showed yielding and necking, as shown in the insert of Figure 3(c). The maximum tensile strength of these composites occurred at yield with the value of 29 MPa to 30 MPa, which was close to that of PBT100. When adding Al particles, the yielding of the PBT/GF/Al composites occurred in a time frame that it moved almost instantaneously toward the breakage of the specimens. This was attributed to the stress concentrators of the Al particles when the PBT-based composites were stretched beyond their yielding. The examples of the tensile fractured specimens are shown in Figure 4. The PBT100 specimens presented necking and whitening before the breakage, while the PBT/GF/Al composites also presented yielding and then breaking toward brittle behavior.

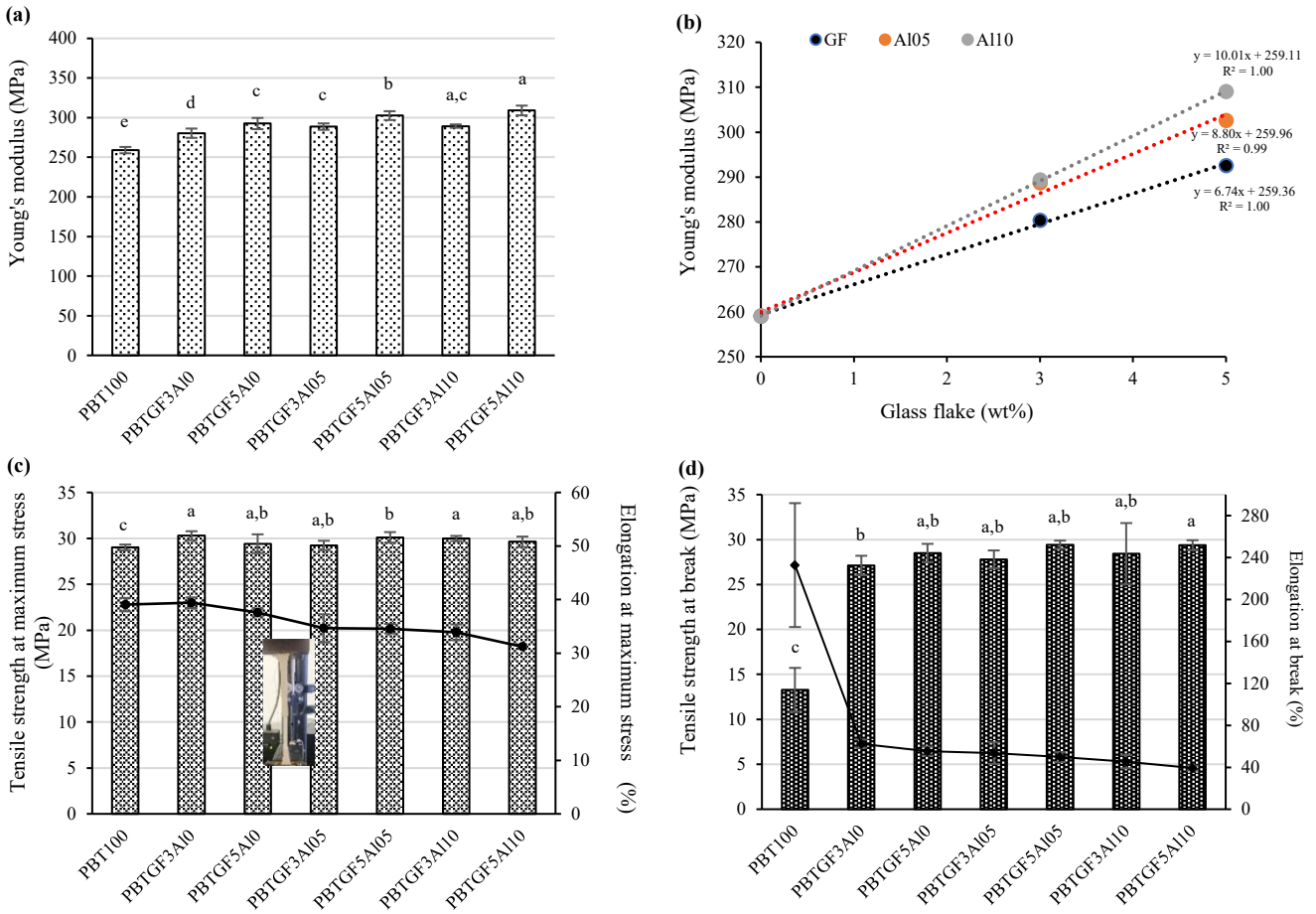

Figure 3. Young's modulus (a,b), tensile strength & elongation at maximum stress (c), and tensile strength & elongation at break (d) of PBT100 and PBT/GF/Al composites.

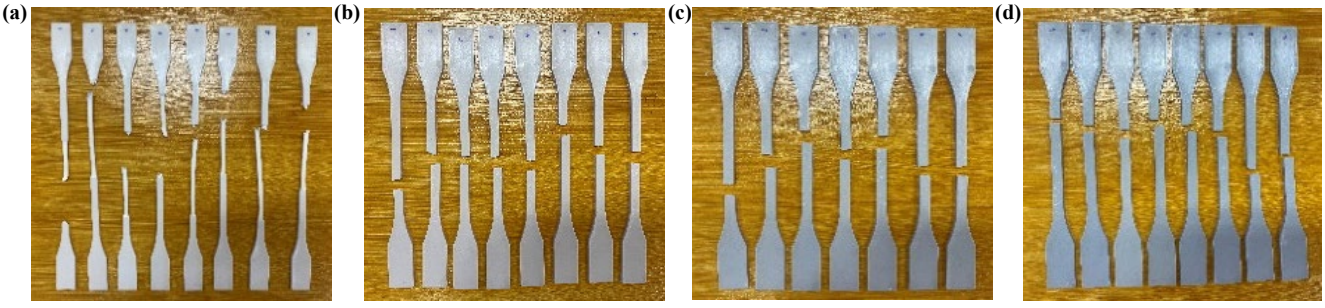

Figure 4. Tensile fractured specimen of PBT100 (a), PBTGF5Al0 (b), PBTGF5Al05 (c), and PBTGF5Al10 (d) composites.

Table 2. Tensile properties of PBT100 and PBT/GF/Al composites.

Abbreviations	Young's modulus [MPa]	Increase of modulus compared with PBT100 [%]	Tensile strength at maximum stress [MPa]	Elongation at maximum stress [%]	Tensile strength at break [MPa]	Elongation at break [%]
PBT100	259.04 ± 4.00^{e}	0.00	29.02 ± 0.31^{c}	39.06 ± 1.26^{a}	13.27 ± 2.45^{c}	232.79 ± 59.08^{a}
PBTGF3Al0	280.37 ± 5.88^{d}	8.24	30.29 ± 0.49^{a}	39.42 ± 1.00^{b}	27.11 ± 1.08^{b}	62.42 ± 3.91^{b}
PBTGF5Al0	292.56 ± 7.10^{c}	12.94	$29.42 \pm 1.03^{a,b}$	37.60 ± 0.73^{b}	$28.49 \pm 1.03^{a,b}$	55.40 ± 4.30^{b}
PBTGF3Al05	288.68 ± 4.05^{c}	11.44	$29.23 \pm 0.51^{a,b}$	$34.66 \pm 2.61^{b,c}$	$27.80 \pm 0.99^{a,b}$	$53.49 \pm 10.27^{b,c}$
PBTGF5Al05	302.58 ± 5.57^{b}	16.81	30.11 ± 0.57^{b}	$34.56 \pm 0.89^{b,d}$	$29.43 \pm 0.45^{a,b}$	$49.73 \pm 4.65^{b,d}$
PBTGF3Al10	$289.33 \pm 2.15^{a,c}$	11.70	29.99 ± 0.28^{a}	$33.89 \pm 1.47^{b,c,d}$	$28.42 \pm 3.42^{a,b}$	$45.33 \pm 6.27^{b,c,d}$
PBTGF5Al10	309.06 ± 6.15^{a}	19.31	$29.63 \pm 0.56^{a,b}$	$31.21 \pm 1.02^{b,c,d}$	29.37 ± 0.55^{a}	39.29 ± 2.3^{c}

Table 3. Flexural properties of PBT100 and PBT/GF/Al composites.

Abbreviations	Flexural modulus [MPa]	Increase (+)/Decrease (-) of flexural moduluscompared with PBT100 [%]	Flexural strength at 5% strain [MPa]
PBT100	$2{,}615.32 \pm 28.18^{d}$	0.00	85.74 ± 0.49^{a}
PBTGF3Al0	$2{,}626.39 \pm 160.34^{c}$	0.42	85.74 ± 3.54^{a}
PBTGF5Al0	$2{,}667.72 \pm 207.18^{b}$	2.00	$84.62 \pm 5.41^{a,b}$
PBTGF3Al05	$2{,}413.62 \pm 87.18^{b,c}$	–7.71	80.87 ± 2.06^{b}
PBTGF5Al05	$2{,}560.65 \pm 40.48^{e}$	–2.09	$82.47 \pm 0.47^{a,b}$
PBTGF3Al10	$2{,}610.89 \pm 78.12^{a,b}$	–0.17	$85.05 \pm 1.81^{a,b}$
PBTGF5Al10	$2{,}709.35 \pm 31.76^{a}$	3.60	$83.67 \pm 0.56^{a,b}$

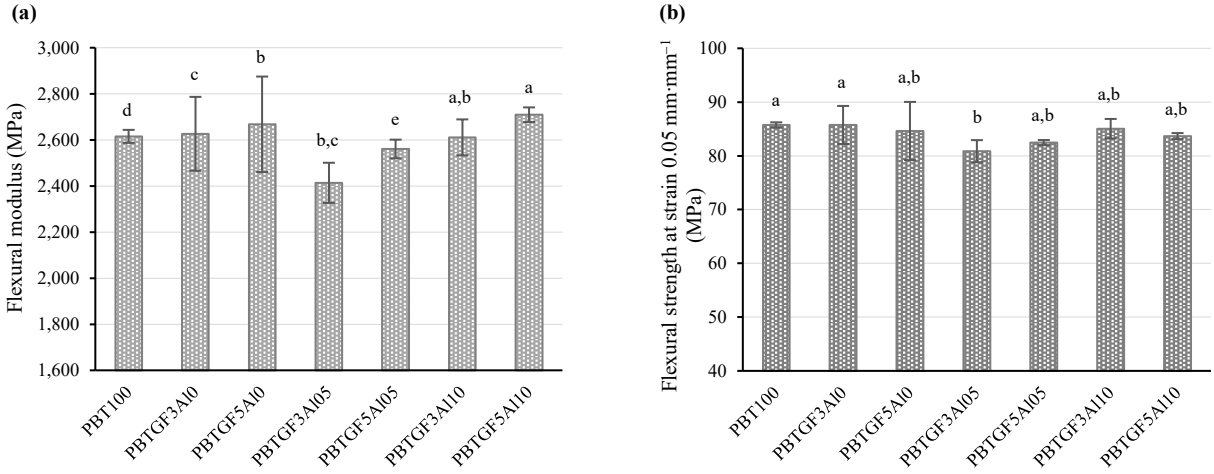

Figure 5. Flexural modulus (a), and flexural strength (b) at strain of 0.05 mm·mm^{-1} of PBT100 and PBT/GF/Al composites.

3.2 Flexural properties of PBT100 and PBT/GF/Al composites

Figure 5 presents flexural modulus and flexural strength at 5% strain of PBT100 and PBT/GF/Al composites, while Table 3 summarizes the values and the percentage of variation that was calculated with the comparison on PBT100 specimens. It is noted that all composite specimens were not broken when the strain reached 5% (0.05 mm·mm^{-1}), and they could recover back to their original shape in a certain amount of time. This implies that these composites withstood flexural stress in elastic behavior within 5% strain. Flexural modulus and flexural strength at 5% strain of the PBT100 were 2,615 MPa and 86 MPa, respectively. Adding GF of 3 wt% or 5 wt% increased the flexural modulus to be 0.42% and 2.00% higher compared to that of PBT100, respectively, and the flexural strength of PBT100 and the PBT/GF composites are in the closed range. This indicates adding GF of just 5 wt% into the PBT matrix did not improve the compressive loading significantly. This would result from the aspect ratio of the GF, which is in the platelet form, not as needle-like as the short glass fiber. Moreover, the interfacial adhesion between the PBT matrix and the GF is limited as shown later in SEM micrographs (Figure 7(a-b)). The load transfer from the polymer matrix into GF might not be sufficient enough to increase the overall stiffness of the composites.

In the presence of Al of 1.0 wt%, the flexural modulus of the PBT/GF/Al composites was higher by about 3.6% compared to that of PBT100. Since these Al particles were not chemically treated to improve the dispersion in the PBT matrix, adding them at 0.5 wt% reduced the flexural modulus of the composites somewhat. This was possibly attributed to the packing of the Al clusters during the 3-point bending that would dissipate the compressive loading via the reduction of free spacing among the Al particles. Mysiukiewicz *et al.* [23] reported the reduction of the elastic modulus of polyethylene by adding Al particles of 1 wt% or 2 wt%, which they compared to the theoretical

and experimental density and concluded that there were fine porosities inside the composites. They discussed extensively that this was related to the agglomeration of Al particles and the inclusion of air inside the Al agglomerates.

3.3 Morphological properties of PBT100 and PBT/GF/Al composites by SEM

Figure 6 shows SEM micrographs of the cryo-fractured surface of PBT/GF/Al composites using the 5,000X magnification. In Figure 6(a), it is seen that the fracture surface of the PBT100 presents the ductile behavior of the polymer matrix, in which the secondary electron (SE) mode highlights the fracture edges that look like zigzagged curves in various levels. From Figure 6(b), the rectangular-like GF is embedded inside the PBT matrix, and the interfacial adhesion between the PBT polyester and the GF is observed due to the chemical compatibility between the PBT polyester and the oxygen species on the glass surface. This confirms how the load transfer could be carried out in the tensile testing to obtain a higher elastic modulus for the PBT/GF composite. However, the interfacial adhesion is limited as the clean surface of the GF is observed when it is peeled cleanly from the PBT matrix, as observed in Figure 6(c). From Figure 6(e-g), the Al cluster was evident as bright spots embedded inside the PBT matrix in the backscattering electron (BSE) mode. As mentioned in the flexural testing, these Al clusters could be packed closer when the composite specimen was compressed [22].

Figure 7 shows SEM micrographs of the tensile-fractured surface of PBT100, PBTGF3Al0, PBTGF5Al0, PBTGF3Al10, and PBTGF5Al10 composites using the 200X magnification. In Figure 7(a), it is seen that the fracture surface of PBT100 is quite rough that indicates the rubbery-state PBT matrix is extended along the tension direction prior to the ductile failure. In Figure 7(b-c), the GF platelets are observed at the fracture surface at which they seem to be peeled off from the PBT matrix leaving the cluster of PBT's thin layers. It is observed that these GFs are not broken into smaller pieces and their surface is clean. This implies the insufficient adhesion between the PBT matrix and the untreated GFs. In Figure 7(d-e), the embedded Al particles are observed as the circular holes on the tensile-fractured surface.

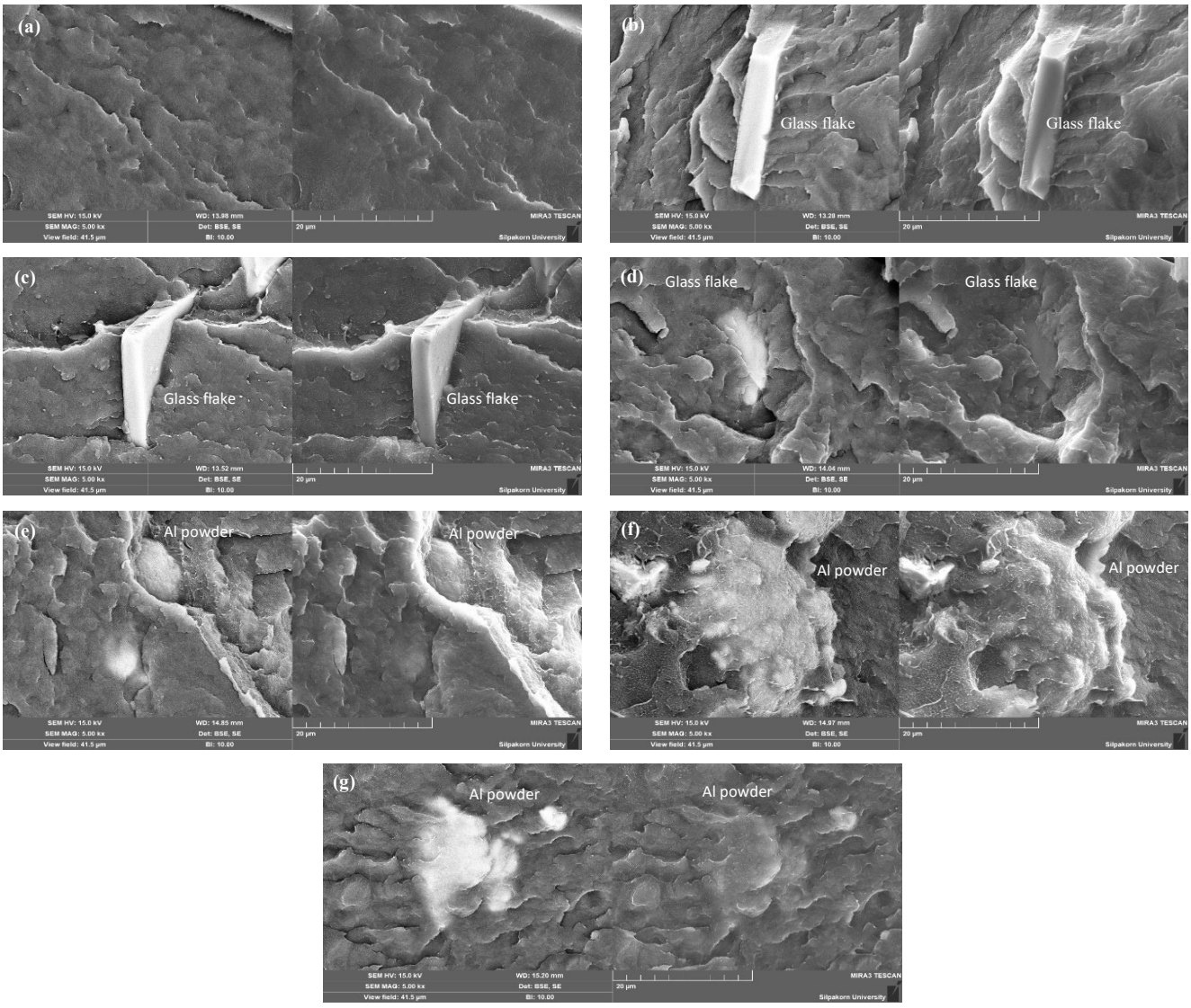

Figure 6. SEM micrographs (at 5,000X magnification) of cryo-fractured surface of PBT100 (a), PBTGF3Al0 (b), PBTGF5Al0 (c), PBTGF3Al05 (d), PBTGF3Al10 (e), PBTGF5Al05 (f), and PBTGF5Al10 (g).

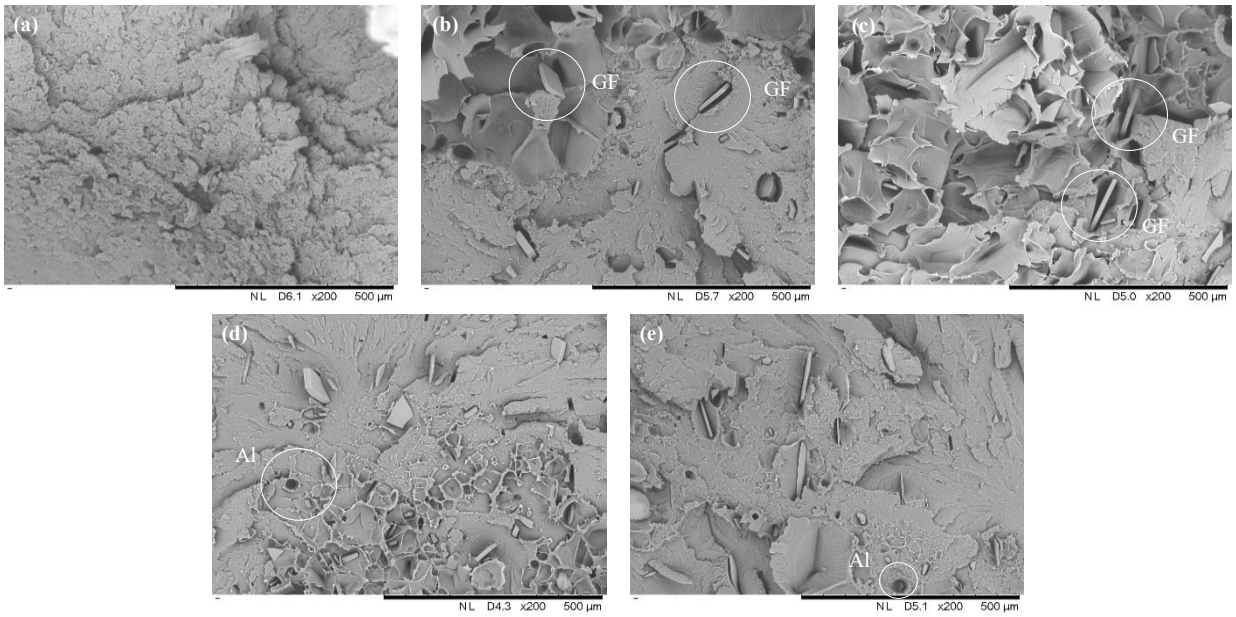

Figure 7. SEM micrographs (at 200X magnification) of tensile-fractured surface of PBT100 (a), PBTGF3Al0 (b), PBTGF5Al0 (c), PBTGF3Al10 (d), and PBTGF5Al10 (e).

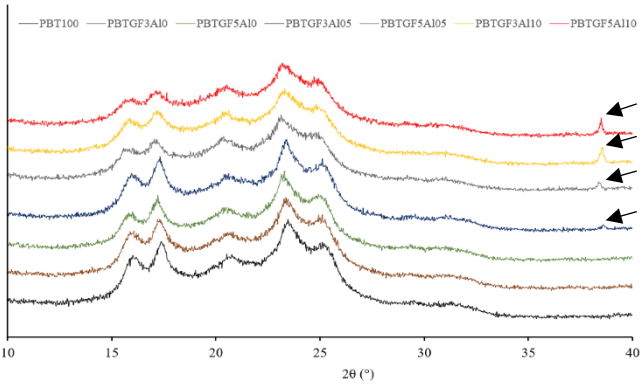

Figure 8. X-ray diffraction (XRD) analysis of the PBT100 and the PBT/GF/Al composites.

3.4 Crystal characteristics of PBT100 and PBT/GF/Al composites by XRD

It is well known that PBT can crystallize in α-form and β-form crystals. The β-form crystals could be obtained by mechanical deformation, and they will be transformed back into α-form crystals when there is no stretching stress [24]. For further crystallization studies, the PBT100 and the PBT/GF/Al composites were characterized by XRD to determine the crystal forms. The samples were cut from the skin of the injection-molded specimens. The XRD patterns are shown in Figure 8. The XRD patterns of the PBT100 and the PBT/GF composites are detected at 2θ = 16.0° (010), 17.4° (010), 20.6° (011), 23.5° (100), and 25.2° (111) which are assigned to the reflections of α-form crystals [6,21]. In addition, for the PBT/GF/Al composites, the small peak at 2θ = 38.5° (111) is assigned to the crystal of Al particles [10,16], which they are pointed with the black arrows in the figure. Clearly, PBT/GF/Al composites exhibit a similar XRD pattern to that of neat PBT, indicating that the incorporation of GF and Al particles do not change the crystal form of PBT.

Table 4 presents the position of the diffraction peaks of PBT100 and PBT/GF/Al composites. Considering the position of 2θ, it is observed that the 2θ is shifted to a few smaller angles in the presence of the fillers. This implies that the crystalline dimensions are larger due to the nucleation effect of the fillers.

Table 5 shows the crystallite dimensions of PBT100 and PBT/GF/Al composites that were calculated from the Scherrer equation. The crystalline dimensions were larger in the [110] and [111] planes with the presence of GF; however, a decreased L_{hkl} corresponding to the [100] implied the preferred growth plane of a lamellae growth direction in the PBT/GF composites. With the presence of Al particles, the crystalline sizes tended to be smaller, which could be observed clearly in the [010] plane for the PBT adding GF of 5 wt%. This phenomenon was explained by Qian *et al.* [21] which this resulted from the heterogeneous nucleation sites from fillers that affected the growth of PBT crystals and could destroy the adjacent spherulitic morphology during the growth process.

3.5 Crystallization characterization of PBT100 and PBT/GF/Al composites by DSC

PBT is a polyester whose butylene segment can crystallize better than the ethylene segment in polyethylene terephthalate (PET). Thus, the degree of crystallinity (X_c) is higher than that of PET and depends on the cooling rate of the molding condition. Haga *et al.* [24] studied extensively about the presence of the mesophase with a liquid crystal-like structure of PBT matrix using XRD, DSC, and ATR-IR. They mentioned that the mesophase occurred from the molecular orientation of the phenylene group of the PBT main chain, and it was not completely amorphous but had a structure with a small endothermic enthalpy of formation. When the PBT100 and PBT/GF/Al composites were studied for crystallization characteristics by DSC, it was found that the 1st heating scan showed only one melting peak while the 2nd heating scan

showed double melting peaks as shown in Figure 9. This implied the influence of the different cooling rates compared between the cooling rate in the injection molding process and the DSC cooling condition.

As specified in the experiment, the DSC samples were cut out from the skin and the core area at the gauge length of the narrow-necked tensile specimen. The objective of this investigation was to determine the influence of the filler on the crystallization. Table 6 summarizes data from the 1st heating, the cooling, and the 2nd heating DSC scans of PBT100 and PBT/GF/Al composites adding GF and Al particles. The only melting peak of the 1st heating scan occurred around 220°C to 221°C. For the PBT100, the X_c at the core area was slightly higher than the value at the skin, while their T_m presented at the same temperature. It implied the core area had a longer cooling time or had the annealing effect due to the low thermal conductivity of the polymer matrix. In contrast, the composites added with GF had significantly higher X_c at the skin area than at the core area, which can be attributed to the nucleation effect of the fillers. With the presence of Al particles, the X_c at the core and the skin area became closer in the values. This could be accredited to the good distribution of the Al particles embedded in the PBT matrix and nucleated the crystallization of the PBT molecules. In the 2nd heating scan, there were double melting peaks and the first melting peak had a much lower enthalpy of fusion (ΔH_m) than that of the second melting peak. Moreover, the presence of the fillers reduced the enthalpy of fusion of the second melting peak and increased the enthalpy of the first melting peak instead. This is attributed to the occurrence of the mesophase of the PBT molecules. This finding is similar to the report by Qian *et al.* [21].

Figure 10 presents the bar chart showing the degree of crystallinity (X_c) of the PBT100 and the PBT/GF/Al composites from the 2nd heating scan, in which the line chart presents the relative ratio of the first X_c to the total X_c (RrX_c,1). These samples were cooled down using a cooling rate of 10°C·min^{-1}, at which there were double melting peaks that occurred at 211° to 214°C (T_m, low) and 220°C to 223°C (T_m, high), respectively. Since there was no cold crystallization during the heating scan, the double peaks indicated the different sizes of the α-form crystals that nucleated and grew under the stress-induced crystallization by the surrounding micro-scale fillers. For the PBT100, the RrX_c,1 was about 14%, and the PBT adding GF of 3 wt% had the increased RrX_c,1 as 21% at both skin and core area. This RrX_c,1 at the core area was increased to 32% when incorporating Al particles of 0.5 wt%, however, the RrX_c,1 was reduced to 20% when the Al content was up to 10 wt%. Interestingly, the PBT adding only GF of 5 wt% had the RrX_c,1 to be 30%, and the RrX_c,1 was reduced to be around 23% in the presence of Al particles. This emphasized the influence of the polar species of the filler surface on nucleation, affecting the crystal form of the PBT molecules. In contrast, the addition of Al particles significantly changed the melting and crystallization of the hydrophobic polyethylene [23].

Figure 11 shows the crystallization temperatures of the PBT100 and the PBT/GF/Al composites from the cooling scan. Adding the GF and Al particles increased the T_c of the PBT matrix, confirming these fillers acted as the nucleating agents. Compared to the T_c of PBT100 of about 188°C, the T_c was shifted to 191°C and 194°C for the GF content of 3 wt% and 5 wt%, respectively. For the PBT adding GF of 3 wt%, the presence of Al particles further increased the T_c to occur at a higher temperature, close to 194°C. For the PBT adding GF of 5 wt%, the presence of Al particles at the skin surface increased the T_c to occur at 196°C. It implies the presence of these particles could nucleate the stress-induced crystallization of the PBT molecules under the injection-molding condition.

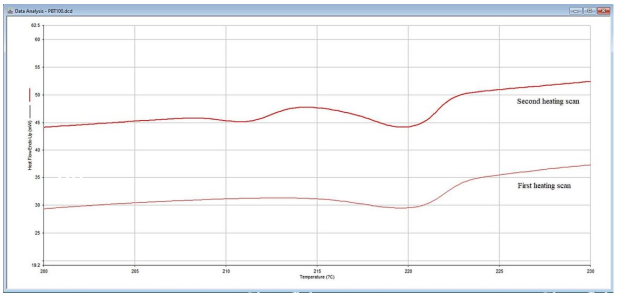

Figure 9. DSC thermograms of the PBT100 samples in the 1st and the 2nd heating scans.

Table 4. The position (2θ) of the diffraction peaks of PBT100 and PBT/GF/Al composites.

hkl	PBT100 [°]	PBTGF3 Al0 [°]	PBTGF5 Al0 [°]	PBTGF3 Al05 [°]	PBTGF5 Al05 [°]	PBTGF3 Al10 [°]	PBTGF5 Al10 [°]
011	16.0	15.9	15.9	16.0	15.5	15.8	15.6
010	17.4	17.3	17.2	17.3	17.0	17.1	17.2
110	20.6	20.5	20.4	20.5	20.3	20.5	20.5
100	23.5	23.4	23.2	23.4	23.1	23.2	23.2
111	25.2	25.1	25.0	25.2	25.1	24.9	25.0

Table 5. Crystallite dimensions of PBT100 and PBT/GF/Al composites.

Samples	L_{011} [nm]	L_{010} [nm]	L_{110} [nm]	L_{100} [nm]	L_{111} [nm]
PBT	13.28	26.61	13.37	31.34	9.43
PBTGF3Al0	23.24	18.62	15.59	20.89	13.47
PBTGF5Al0	13.28	53.22	15.59	26.85	26.94
PBTGF3Al05	23.24	15.52	15.59	26.86	11.79
PBTGF5Al05	30.97	31.03	18.70	62.64	11.79
PBTGF3Al10	13.28	15.52	18.71	11.75	15.71
PBTGF5Al10	23.23	15.52	11.70	37.59	11.79

Table 6. Data from the 1st heating, the cooling and the 2nd heating DSC scans showing crystal melting temperatures (T_m), enthalpy of fusion (ΔH_m), crystallization temperature (T_c), and the degree of crystallinity (X_c) of PBT100 and PBT/GF/Al composites.

Abbreviations	1st heating scan		Cooling	2nd heating scan					
	T_m [°C]	X_c [%]	T_c [°C]	$T_{m,1}$ [°C]	$T_{m,2}$ [°C]	$\Delta H_{m,1}$ [J·g^{-1}]	$\Delta H_{m,2}$ [J·g^{-1}]	$X_{c,1}$ [%]	$X_{c,2}$ [%]
PBT100 skin	221.0	29.1	188.3	210.8	220.5	5.075	33.505	3.63	23.93
PBT100 core	221.0	31.4	188.6	211.2	220.7	5.915	33.367	4.23	23.83
PBTGF3Al0 skin	220.8	36.8	191.0	212.3	221.1	7.792	28.613	5.40	19.82
PBTGF3Al0 core	220.8	31.7	190.8	212.1	221.2	7.983	29.364	5.53	20.35
PBTGF5Al0 skin	221.6	35.5	194.3	214.5	223.0	5.839	16.438	3.96	11.15
PBTGF5Al0 core	220.7	30.0	194.2	214.3	222.0	8.031	17.059	5.45	11.58
PBTGF3Al05 skin	220.6	27.6	191.6	212.0	220.5	7.652	27.911	5.30	19.33
PBTGF3Al05 core	220.3	30.5	191.9	212.6	221.2	6.487	26.556	4.49	18.39
PBTGF5Al05 skin	221.0	33.7	195.7	212.9	220.5	10.544	24.621	7.15	16.70
PBTGF5Al05 core	221.3	29.3	194.5	213.7	221.5	8.943	20.864	6.07	14.15
PBTGF3Al10 skin	221.0	35.3	193.2	212.6	220.7	8.213	26.039	5.68	18.02
PBTGF3Al10 core	220.8	34.2	193.5	213.3	221.6	8.345	25.525	5.78	17.67
PBTGF5Al10 skin	221.0	34.6	193.2	212.6	220.7	7.894	26.039	5.35	17.65
PBTGF5Al10 core	220.8	35.1	193.5	213.3	221.6	8.345	25.525	5.66	17.30

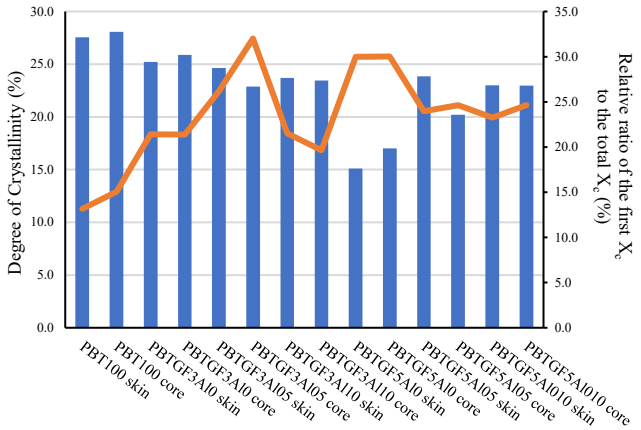

Figure 10. Degree of crystallinity (X_c) of the PBT100 and the PBT/GF/Al composites from the 2nd heating scan. The line curve is the relative ratio ($RrX_{c,1}$) of the first X_c to the total X_c.

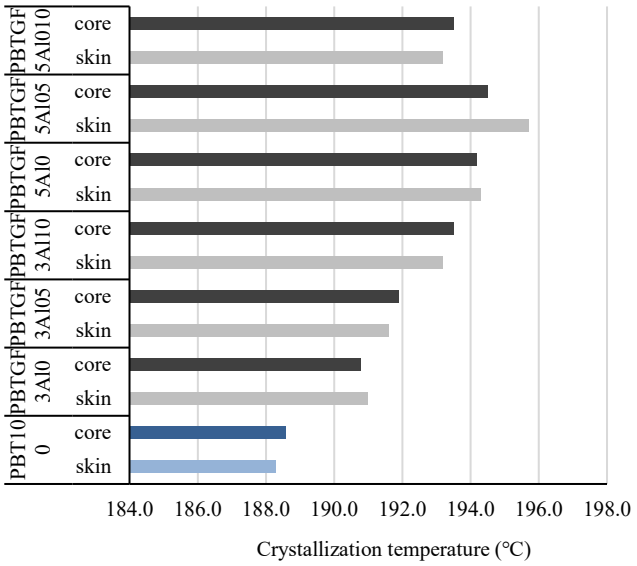

Figure 11. Crystallization temperatures of the PBT100 and the PBT/GF/Al composites.

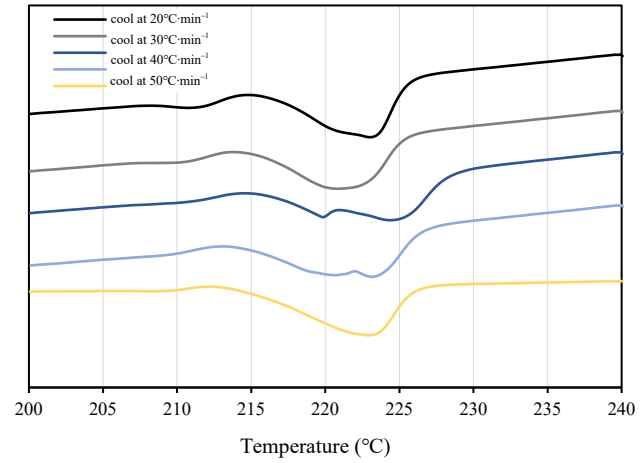

Figure 12. Melting scans of the PBT100 and the PBT-based composites after erasing thermal history using different cooling rates.

3.6 Non-isothermal crystallization of PBT100 and PBT/GF/Al composites by DSC

Figure 12 presents the heating scans after erasing thermal history rapidly and cooling at cooling rates of 20°C·min^{-1} to 60°C·min^{-1}. It was found that the PBT100 and the PBT/GF/Al composites had similar melting thermograms. The overlapping or the splitting melting curves depended on the cooling rates after erasing thermal history. The melting thermogram occurred as double endothermic peaks after being subjected to a cooling rate of 20°C·min^{-1} and 30°C·min^{-1}. The melting thermogram occurred as two partially overlapping endothermic peaks after being subjected to a cooling rate of 40°C·min^{-1} and 50°C·min^{-1}. The melting thermogram after being subjected to a cooling rate of 60°C·min^{-1} occurred as one endothermic peak. The overlapping endothermic peaks occurred at two neighboring T_m, with the higher melting temperature related to the crystallization of the α-form crystals, and subsequently the thinner crystals or the imperfect crystals crystallized at a lower melting temperature. Heidrich and Gehde [25] explained the presence of the double melting peaks of the PBT using the three-phase

model. In this model, any semi-crystalline thermoplastics consists of a mobile amorphous fraction (MAF), a rigid amorphous fraction (RAF), and a crystalline fraction (CF). The double melting peaks of PBT could gradually merge into one single melting temperature when the PBT crystallizes at a high crystallization temperature for non-isothermal crystallization study. After passing the primary and the secondary crystallization, the initial mobile amorphous phase could be converted into both the rigid amorphous phase and the crystalline phase over a long period of time. This is possibly due to the rearrangement of the phenylene groups in the backbone of aliphatic PBT molecules that changes from the rigid amorphous phase to be the crystalline phase when the cooling rate is slow.

From the processing point of view, the cooling rate of the injection-molded PBT/GF/Al specimens was faster than 60°C·min^{-1}, considering the difference between the nozzle temperature (260°C) and the mold temperature (80°C), and the cooling time was 30 s. Although the fillers could act as nucleating agents for the crystallization, the cooling rate was so fast that the PBT molecules crystallized in the α-form with different crystal sizes. The deformation during the flow in the relatively cold mold caused these crystals to nucleate and grow heterogeneously. The β-form crystals that could form by the stress-induced orientation of the liquid crystal-like structure was not observed in the injection-molded specimens using the combination of the setting injection velocity and the mold temperature.

Figure 13 shows crystallization temperatures (T_c) of PBT100 and PBT/GF/Al composites when cooling down at various cooling rates. It is seen that the T_c was the highest when the samples were cooled down at the lowest cooling rate. The finding is similar to the report by Liu and Wu [26]. They reported that the increased cooling rate shifted the crystallization toward lower temperatures and also broadened the crystallization peak. This indicated that when the polymer melt was cooled down at a slower cooling rate, the crystallization began at a higher temperature. In other words, the polymer molecules had a longer time that was sufficient enough for them to nucleate at a higher temperature, and then other adjacent molecules started crystal forming. In the presence of GF, the polymer molecules could interact with oxygen atoms on the filler surface and then nucleate the crystallization at higher temperatures. Thus, the T_c at the cooling rate of 20°C·min^{-1} was shifted from that of neat PBT at 183°C to 186°C and 190°C when adding GF of 3 wt% and 5 wt%, respectively. In the presence of fine Al particles, the T_c was shifted further to higher temperatures due to the good distribution of Al particles inside the PBT matrix. In comparison between the GF and Al particles, the nucleation effect of GF on the PBT molecules seemed to be more affected than that of the Al particles. This is in contrast with the report by Hsu-I Mao *et al.* [27]. They studied the non-isothermal DSC of PBT-co-PTMEG copolymers in a temperature range from 50°C to 24°C under 2°C·min^{-1}, 5°C·min^{-1}, 10°C·min^{-1}, and 20°C·min^{-1}. They reported that the exothermic peaks of the copolymers shifted to a lower temperature as the cooling rate increased, demonstrating that the incorporation with PTMEG hindered the PBT molecular chains from packing into an ordered state.

3.7 Electrical surface resistivity of PBT100 and PBT/GF/Al composites

One of the main important characteristics of this kind of composite is its electrical properties. Electrical surface resistance is defined as a resistance to leakage of electricity along the surface of a material. Table 7 presents the electrical surface resistivity of PBT100 and the PBT/GF/Al composites. It was found that adding GF of 5 wt% reduced the electrical surface resistivity of the PBT matrix from 10^{11} ohm·sq^{-1} to 10^{10} ohm·sq^{-1}. For the Al-added PBT composites, the electrical surface resistivity was still in the range of 10^{10} ohm·sq^{-1} for either the concentration of 0.5 wt% or 1.0 wt%. This indicates that adding the hybrid GF/Al fillers of about 6 wt% into the PBT matrix produces the anti-static polymeric composite. The current classifications for electrical surface resistivity per EIA-541 and other specifications [28] is that a conductive material should have the electrical surface resistivity less than 10^5 ohm·sq^{-1}, a dissipative material should have the electrical surface resistivity between 10^5 ohm·sq^{-1} and 10^{12} ohm·sq^{-1}, and an insulative materials should have the electrical surface resistivity above 10^{12} ohm·sq^{-1}. Also, the TE connectivity [29] specifies that an antistatic material should have a surface resistivity equal to or greater than 1×10^5 ohm·sq^{-1} but less than 1×10^{12} ohm·sq^{-1}.

Table 7. Electrical surface resistivity measurement of PBT100 and PBT/GF/Al composites.

Abbreviations	Electrical surface resistivity [ohm·sq^{-1}]
PBT100	~10^{11}
PBTGF3Al0	~10^{11}
PBTGF5Al0	~10^{10}
PBTGF3Al05	~10^{10}
PBTGF5Al05	~10^{10}
PBTGF3Al10	~10^{10}
PBTGF5Al10	~10^{10}

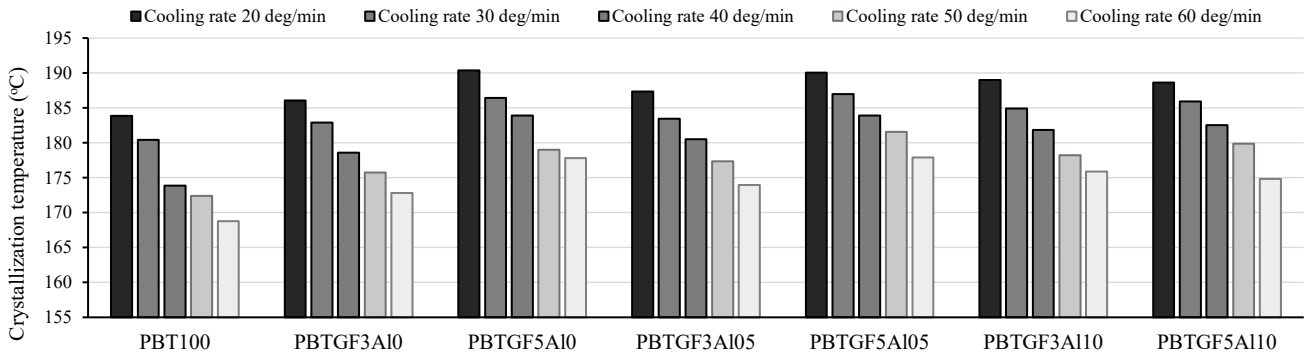

Figure 13. Crystallization temperatures of PBT100 and PBT/GF/Al composites from non-isothermal DSC studies.

4. Conclusions

In this research, the PBT matrix was melt-compounded with a hybrid filler of GF of 3 wt% or 5 wt% and Al particles of 0.5 wt% or 1.0 wt%. The PBT/GF 3 wt% composites with Al particles of 0.5 wt% and 1.0 wt% had Young's modulus of 11.44% and 11.70% higher than neat PBT. The PBT/GF 5 wt% with Al particles of 0.5 wt% and 1.0 wt% had Young's modulus of 16.81% and 19.31% higher than neat PBT. The stress-strain curves of the PBT adding GF of 3 wt% or 5 wt% showed yielding and then necking, similar to neat PBT, with the maximum tensile strength of 29 MPa to 30 MPa. Moreover, in the presence of the Al particles, the tensile strength at yield and at break of the PBT/GF composites occurred at almost the same point due to the stress concentration of distributed Al particles. Adding GF of 3 wt% or 5 wt% increased the flexural modulus of the composites to be 0.42% and 2.00% higher than that of neat PBT, respectively. Flexural strength at 5% strain of PBT100 and the PBT/GF composites was in the closed range, with the flexure specimens recovering back elastically to the original shape after a certain time. In the presence of Al of 1.0 wt%, the flexural modulus of the PBT/GF/Al composites was increased to be about 3.6% higher compared to that of neat PBT. From XRD analysis, the neat PBT and all PBT/GF/Al composites exhibited similar XRD patterns of α-form crystals. It is observed that the increased crystal dimensions in the [110] and [111] planes were increased, implying the heterogeneous nucleation with the presence of these fillers. From DSC analysis, adding the GF and Al particles increased the T_c of the PBT matrix, confirming these fillers acted as the nucleating agents. The single peak of the crystal melting temperatures occurred at 220°C to 221°C for the injection-molded specimens, and the crystal melting temperature occurred as double peaks when the cooling rate was slower than 60°C·min^{-1}. However, the X_c did not differ significantly because of these fillers. The influence of the injection velocity and the mold temperature should be further investigated since the crystallization of the PBT composites might be increased and enhance mechanical properties. Finally, adding GF/Al fillers of about 6 wt% reduced the electrical surface resistivity to 10^{10} ohm·sq^{-1}, which the proper chemical treatment of the aluminum particles possibly further reduces the electrical surface resistivity.

Acknowledgements

This research was financially supported by the Department of Materials Science and Engineering, Faculty of Engineering and Industrial Technology, Silpakorn University. Mr. Piroch Tangsupatawat was thankful for his help with the injection molding machine.

References

[1] M. Vosough Kia, M. Ehsani, S. E. Hosseini, and G. H. Asadi, "Fabrication and characterization of transparent nanocomposite films based on poly (lactic acid)/polyethylene glycol reinforced with nano glass flake," *International Journal of Biological Macromolecules*, vol. 254, p. 127473, 2024.

[2] P. Russo, F. Cimino, D. Acierno, G. Lupò, and C. Petrarca, "Poly(butylene terephthalate) based composites containing alumina whiskers: Influence of filler functionalization on dielectric properties," *International Journal of Polymer Science,* vol. 2014, p. 9, 2014.

[3] N. G. Karsli, C. Ozkan, A. Aytac, and V. Deniz, "Characterization of poly(butylene terephthalate) composites prepared by using various types of sized carbon fibers," *Materials and Design*, vol. 87, pp. 318–323, 2015.

[4] Z. Yenier, S. Aker, Y. Seki, L. Altay, O. Bigun, and M. Sarikanat, "Improving thermal conductivity of polybutylene terephthalate composites with hybrid synthetic graphite and carbon fiber," *Journal of Thermoplastic Composite Materials*, vol. 36, no. 2, 2023.

[5] M. Yokouchi, Y. Sakakibara, Y. Chatani, H. Tadokoro, T. Tanaka, and K. Yoda, "Structures of two crystalline forms of poly (butylene terephthalate) and reversible transition between them by mechanical deformation," *Macromolecules*, vol. 9, no. 2, pp. 266–273, 1976.

[6] S. Colonna, R. A. Perez-Camargo, H. Chen, G. Liu, D. Wang, A. J. Müller, G. Saracco, and A. Fina, "Supernucleation and orientation of poly(butylene terephthalate) crystals in nano-composites containing highly reduced graphene oxide," *Macromolecules*, vol. 50, pp. 9380−9393, 2017.

[7] GlassFlakes. https://www.glassflakes.com/specification/ (accessed 3 January, 2024).

[8] C. J. Watkinson, and J. H. K. Elvidge, "Method and apparatus for forming glass flakes," England, 1987.

[9] S. Jharimune, X. Gu, M. L. Lim, M. Dent, N. Rakers, C. Y. Lee, H. He, A. Mubarok, and C. B. Hui, "Effect of glass flake in anti-corrosive coatings for extreme conditions," presented at the AMPP Annual Conference + Expo, San Antonio, Texas, USA, 2022. [Online]. Available: https://onepetro.org/amppcorr/ proceedings-abstract/AMPP22/2AMPP22/D021S010R002/488835.

[10] A. Alhamidi, A. Anis, S. M. Al-Zahrani, Z. Bashir, and M. M. Alrashed, "Conductive plastics from Al platelets in a PBT-PET polyester blend having co-continuous morphology," *Polymers*, vol. 14, no. 6, p. 1092, 2022.

[11] E. Alagöz, and E. Selver, "Glass flakes for enhancing mechanical properties of glass/epoxy composites," *Proceedings of the Institution of Mechanical Engineers, Part L: Journal of Materials: Design and Applications*, vol. 238, no. 8, pp. 1438–1456, 2024.

[12] M. E. Fatemeh S. Miri, Hossein A. Khonakdar, and Behjat Kavyani, "A comprehensive study on physical, mechanical, and thermal properties of poly(ethylene terephthalate) filled by micro- and nanoglass flakes," *Journal of Vinyl and Additive Technology*, vol. 26, no. 3, pp. 380–389, 2020.

[13] I. Kobykhno, A. Kiryanov, V. Klinkov, A. Chebotareva, S. Evlashin, D. Ju, Y. Wu, A. Semencha, H. Zhao, and O. Tolochko, "Effect of glass filler geometry on the mechanical and optical properties of highly transparent polymer composite," *Polymers*, vol. 14, no. 23, p. 5179, 2022.

[14] T. Michii, M. Seto, M. Yamabe, Y. Kubota, G. Aoki, and H. Ohtsuka, "Study on warpage behavior and filler orientation during injection molding," *International Polymer Processing*, vol. 23, no. 5, pp. 419–429, 2008.

[15] N. Vidakis, M. Petousis, N. Mountakis, V. Papadakis, C. Charou, V. Rousos, and P. Bastas, "Glass fillers in three different forms used as reinforcement agents of polylactic acid in material

extrusion additive manufacturing," *Applied Science*, vol. 13, pp. 6471-6496, 2023.

[16] A. Anis, A. Y. Elnour, M. A. Alam, S. M. Al-Zahrani, F. AlFayez, and Z. Bashir, "Aluminum-filled amorphous-PET, a composite showing simultaneous increase in modulus and impact resistance," Polymers, vol. 12, p. 2038, 2020.

[17] S. Yang, Q. Wang, and B. Wen, "Highly thermally conductive and superior electrical insulation polymer composites via in situ thermal expansion of expanded graphite and in situ oxidation of aluminum nanoflakes," *ACS Applied Materials & Interfaces*, vol. 13, no. 1, pp. 1511–1523, 2021.

[18] A. F. Osman, and M. Mariatti, "Properties of aluminum filled polypropylene composites," *Polymers and Polymer Composites*, vol. 14, no. 6, pp. 623–633, 2006.

[19] S. A. Vyavahare, B. M. Kharat, and A. P. More, "Polybutylene terephthalate (PBT) blends and composites: A review," *Vietnam Journal of Chemistry*, vol. 62, no. 5, pp. 1–11, 2023.

[20] C. Loyer, P. Ferreira, J.-B. Marijon, V. Michel, G. Regnier, J. Vera, V. Duval, and E. Richaud, "Embrittlement of polybutylene terephthalate induced by injection molding," *Polymer Degradation and Stability*, vol. 196, p. 109843, 2022.

[21] P. Qian, Y. Zhang, H. Mao, H. Wang, and H. Shi, "Nucleation and mechanical enhancements in poly(butylene terephthalate) nanocomposites influenced by functionalized graphene oxide," SN Applied Sciences, vol. 1, p. 443, 2019.

[22] O. Hamlaoui, O. Klinkova, R. Elleuch, and I. Tawfiq, "Effect of the glass fiber content of a polybutylene terephthalate reinforced composite structure on physical and mechanical characteristics," *Polymers,* vol. 14, p. 17, 2022.

[23] O. Mysiukiewicz, P. Kosmela, M. Barczewski, and A. Hejna, "Mechanical, thermal and rheological properties of polyethylene-based composites filled with micrometric aluminum powder," *Materials*, vol. 13, no. 5, p. 1242, 2020.

[24] M. Haga, T. Nakaoki, H. Ishihara, K. Yamashita, and K. Funaki, "Crystallinity and chain orientation of injection-molded poly (butylene terephthalate) depending on the depth profile at the surface," *Trends in Chemical Engineering*, vol. 17, pp. 1–9, 2019.

[25] D. Heidrich, and M. Gehde, "The 3-phase structure of polyesters (PBT, PET) after isothermal and non-isothermal crystallization," *Polymers*, vol. 14, p. 793, 2022.

[26] B. Liu, and W. Wu, "Nonisothermal crystallization kinetics of poly(butylene terephthalate)/epoxidized ethylene propylene diene rubber/glass fiber composites," *Polymer Engineering & Science*, vol. 59, no. 2, pp. 217–434, 2019.

[27] H.-I. Mao, C.-W. Chen, and S.-P. Rwei, "Synthesis and non-isothermal crystallization kinetics of poly(butylene terephthalate-co-tetramethylene ether glycol) copolyesters," *Polymers*, vol. 12, no. 9, p. 1897, 2020.

[28] R. Nisticò, M. D'Arienzo, B. D. Credico, S. Mostoni, and R. Scotti, "The role of inorganic fillers in electrostatic discharge composites," *Inorganics*, vol. 10, p. 222, 2022.

[29] TE_Connectivity. "Requirements for electrostatic protective packaging material." https://www.te.com/commerce/DocumentDelivery/DDEController?Action=srchrtrv&DocNm=115-59&DocType=Specification+Or+Standard&DocLang=English&PartCntxt= 2324869-2&DocFormat=pdf (accessed 07/17/2025, 2025).